Testing the Effectiveness of Wavelet-based Denoising Schemes for Gear Fault Diagnosis

Mustapha MERZOUG
Laboratoire de Mécanique Avancée, USTHB, BP 32 El Alia 16111 Bab Ezzouar, Algérie, mmerzoug@usthb.dz

Abstract: - Vibration analysis has always been used for the diagnosis of gear faults. The vibration signals obtained are generally contaminated with noise and therefore not usable. The denoising of the vibration signals obtained helps in the diagnosis of faults, giving significant results. The wavelet transform increases the signal-to-noise ratio, reduces the mean absolute error, and is recommended for denoising gear vibration signals. The extracted signals must be denoised by choosing an appropriate denoising scheme to preserve the information contained in the signal. An approach has been developed in this work to show the effectiveness of this method. We chose a single-stage dynamic model with basically two shafts, one driving a load and the other a motor, to obtain this signal. Four bearings and two gears support both shafts. The meshing stiffness and the response have been calculated by an analytical method and a Newmark integration scheme, respectively. Then, we deliberately introduced a defect in the shape of a crack in a gear tooth. We selected Daubchies wavelets, which are well adapted to this type of problem. The objective is to control the different parameters related to our approach based on the wavelet transform, which is the levels of decomposition and the order of the wavelets. This approach consists of observing a series of indicators for a series of wavelet orders depending on the severity of the defect. The novelty of this research work is the improvement of scalar indicators while mastering the parameters linked to the wavelet transform. Our approach has been compared to other well-known methods in the literature.

Keywords: - Spur gear; Vibration analysis, Denoising, Wavelet transform, Kurtosis, Crest factor.

1. INTRODUCTION

Gear transmissions are mechanical components widely used in industries. A gear failure results in damage to the gearbox as well as machine components. Failure can result in significant production losses as well as high maintenance costs and safety problems. [1]. Gears made up of teeth are subject to certain degradations. Tooth cracking is an undesirable phenomenon that can cause serious and costly damage. The variation of the meshing stiffness over time is the main reason for gear vibrations [2]. Many studies have been conducted on the evaluation of mesh stiffness. FEM and the analytical method (AM) have been and are still applied to calculate the mesh stiffness [3, 4]. In their paper [5], an analytical FEM model is developed to calculate the time-varying mesh stiffness of spur gear pairs with a complex foundation and a crack. The pinion and gear foundations are simulated as cylinders and modeled by three-dimensional finite elements. The tooth pair is equivalent to a spring, and the mesh stiffness of a tooth pair is obtained by the potential energy method. Zhiguo et al. [6] calculated the mesh stiffness of spur gears through the potential energy method by considering bending, axial compressive, and Hertzian energy.

The effect of crack size on mesh stiffness is studied by Wang [7]. Yang et al. [8] highlighted this effect on the dynamic response of gear transmission. Pandya and Parey [9, 10] evaluated the effect of the crack path on the mesh stiffness as a function of different gear parameters, such as pressure angle, fillet radius, and contact ratio.

Many signal processing methods have been proposed in the literature to detect faults in gear drives. In their paper, Tayachi et al. [11], they first adopt wavelet theory to remove noise, and then use the empirical mode decomposition characteristics of the Hilbert-Huang transform, to analyze useful intrinsic mode functions (IMFs) based on signal modulation and correlation theory.

The problem of strong noise components masking the essential information of the signals has always posed challenges for engineers in the field of machine condition monitoring. Several wavelet-based signal processing techniques aimed at denoising the signal obtained to increase the Signal-to-Noise Ratio (SNR) and reduce the Root Mean Square Error (RMSE) have been proposed and tried by several researchers [12–15].

During signal processing, the noise must be eliminated and the real signal must be taken for analysis. The Wavelet Transform (WT) is one of the most powerful approaches to de-noise the signal since the decomposition and reconstruction of the signal are done in such a way that the result contains the essential information.

This work claims to use the WT to compare the performances of two adopted approaches: denoising schemes (Empirical Mode Decomposition EMD and Spectral Subtraction), and a widely used denoising scheme (WT) for denoising gear vibration signals. These schemes were compared using SNR, Kurtosis, and RMSE. The best denoising scheme is based on the ability to identify defects.

2. DYNAMIC MODELING

The adopted dynamic model for a pair of gears is composed of four disks representing the inertia of the gears, driver, and load. Springs represent meshing stiffness, torsional stiffness, and flexural stiffness. This model has the particularity of being extended to include other effects (e.g., variable meshing stiffness and damping, friction, gearing errors, etc.). In addition, it includes other components.

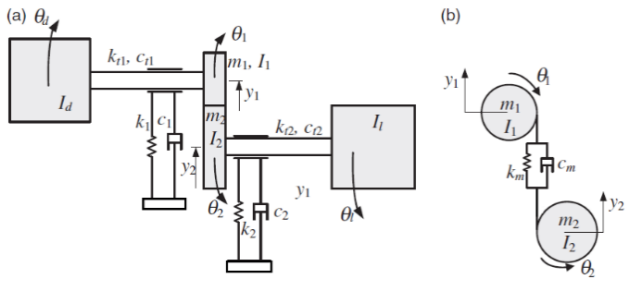

Figure 1. The dynamic model of a reduction gear system [16]

2.1. Equations of Motion

The dynamic response of the gear transmission can be extracted from the dynamic model. A dynamic simulation was undertaken based on the time-varying mesh stiffness model using a Newmark integration scheme. Figure 1 shows the selected dynamic model, and the dynamic equations governing this system are derived as in Eqs. (1)-(7).

$$I_d\ddot{\theta}_d + C_{t1}\left(\dot{\theta}_d - \dot{\theta}_1\right) - K_{t1}\left(\theta_d - \theta_1\right) = T_d \quad (1)$$

$$I_1\ddot{\theta}_1 + C_{t1}\left(\dot{\theta}_1 - \dot{\theta}_d\right) + K_{t1}\left(\theta_1 - \theta d\right) = -R_1.F_y \quad (2)$$

$$I_2\ddot{\theta}_2 + C_{t2}\left(\dot{\theta}_2 - \dot{\theta}_l\right) + K_{t2}\left(\theta_2 - \theta_l\right) = R_2.F_y \quad (3)$$

$$I_1\ddot{\theta}_1 + C_{t2}\left(\dot{\theta}_1 - \dot{\theta}2\right) - K_{t2}\left(\theta_1 - \theta_2\right) = -T_1 \quad (4)$$

$$m_1\ddot{y}_1 + C_1\left(\dot{y}_1 - \dot{y}_3\right) + K_1\left(y_1 - y_3\right) = F_y \quad (5)$$

$$m_2\ddot{y}_2 + C_2\left(\dot{y}_2 - \dot{y}_4\right) + K_2\left(y_2 - y_4\right) = -F_y \quad (6)$$

where F_y is the dynamic meshing force given by:

$$F_y = C_m\left(R_1\dot{\theta}_1 - R_2\dot{\theta}_2 + \dot{y}_2 - \dot{y}_1\right) + K_m\left(R_1\theta_1 - R_2\theta_2 + y_2 - y_p\right) \quad (7)$$

The equations of motion can be arranged in matrix form as follows:

$$M\ddot{X} + C\dot{X} + KX = F \quad (8)$$

where the system displacement vector is arranged as follows:

$$X = \left[\theta_d\ \theta_1\ \theta_2\ \theta_l\ y_1\ y_2\ \right] \quad (9)$$

The matrices M, C, and K are the diagonal inertia matrix, the damping matrix, and the stiffness matrix, respectively. It is noted that the force vector F considers the driving torque, the load torque, and the excitations of the gearing due to gearing errors.

The transmission parameters used in all simulations are shown in Table 1.

Table 1. Parameters of the gear-pinion dynamic model

Pinion mass, m_1, (Kg)	0.377
Gear mass, m_2, (Kg)	0.512
Pinion mass moment of inertia, I_1, (Kg.m^2)	0.96 10^{-4}
Gear mass moment of inertia, I_2, (Kg.m^2)	1.98 10^{-4}
Drive mass moment of inertia, I_d, (Kg.m^2)	0.0015
Load mass moment of inertia, I_l, (Kg.m^2)	0.0035
Torsional stiffness K_{t1} and K_{t2}, (N.m/rad)	4.4 10^4

Each shaft's transverse stiffness is modeled as one spring attached to the bearing, K_1 and K_2. The estimated stiffness parameters are, therefore, given by:

$K_1 = 6.56\ 10^7$ N/m $K_2 = 6.56\ 10^7$ N/m

2.2. Crack Modelling and Gear Mesh Stiffness Calculations

Gear transmissions are affected by operating conditions such as excessively applied loads, improper lubrication, and manufacturing errors. A high concentration of stresses can be produced in the meshing gear teeth; a crack can occur and start to propagate during operation.

The dynamic behavior of a gear transmission is affected by the status of the engaged gear teeth. One of the most important reasons for the vibration and dynamic excitation of gears is the variation of the stiffness of the mesh with time [17].

In the current section, an analytical approach is applied, which was previously described by Chen and Shao [18], for evaluating the time-varying gear mesh stiffness.

The crack modeling required for stiffness calculations is illustrated in Figure 2.

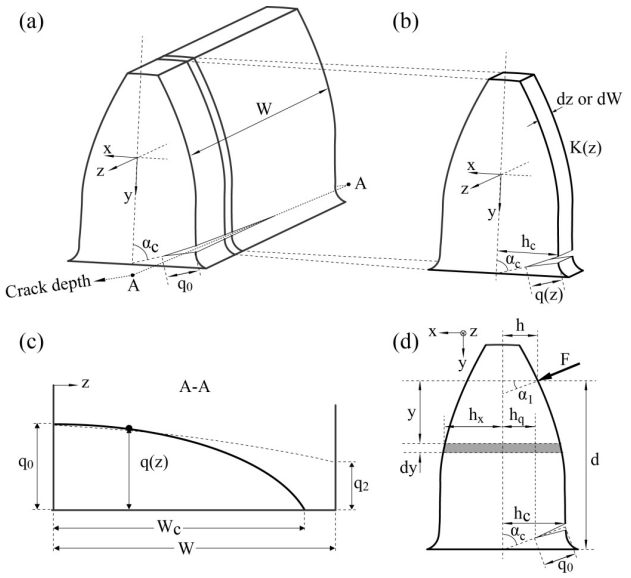

Figure 2. Modeling of a gear tooth crack: (a) modeling of a cracked tooth, (b) modeling of one slice of width dW, (c) crack depth distribution along the tooth width, and (d) tooth notation [17]

The tooth is considered a non-uniform cantilever beam with an effective length d (see Figure 2d), and the mesh stiffness can be calculated after the deflections under the action of a force are determined. Note that in this part of the stiffness calculations, it is assumed that the crack has a constant depth, q(z), for each slice, dW, along the tooth width, as explained in Figures 2a and 2b. Based on the calculation of the potential energy stored in a gear tooth, it is possible to trace the flexural, shear, and axial compression stiffness.

$$\frac{1}{K_b} = \int_0^d \frac{\left(x\cos(\alpha_1) - h\sin(\alpha_1)\right)^2}{EI_x} \tag{10}$$

$$\frac{1}{K_s} = \int_0^d \frac{1.2\cos^2(\alpha_1)}{GA_x} \tag{11}$$

$$\frac{1}{K_a} = \int_0^d \frac{\sin^2(\alpha_1)}{EA_x} \tag{12}$$

where the following notations are used:

K_b: Bending stiffness.

K_s: Shear stiffness.

K_a: Axial compressive stiffness.

h, h_c, h_x, x, dx, d, and α_1 are illustrated in Figure 2d. Note that α_1 varies with the gear tooth position.

E: Young's modulus.

G: Shear modulus, $G = \frac{E}{2(1+\nu)}$.

ν: Poisson ratio.

I_x: Area moment of inertia.

q(z) and α_c are the crack depth and crack angle, respectively, as shown in Figure 2b.

At a certain position, 'z', through the tooth width, we can find the stiffness of one slice resulting from the effect of all the stiffnesses calculated previously as follows:

$$K(z) = 1/\left(\frac{1}{K_b} + \frac{1}{K_s} + \frac{1}{K_a}\right) \tag{13}$$

The mesh stiffness model presented in [18] divides the tooth width into thin slices to represent the crack propagation through the tooth width, as shown in Figure 2a. Consequently, for a small dW, the crack depth is assumed to be constant through the width of each slice; see Figure 2b.

By integrating the stiffness of all the slices along the width, the stiffness of the entire tooth can be evaluated as follows:

$$K_{tp} = \int_0^W K(z) \tag{14}$$

In [18], it is assumed that the distribution of the crack depth follows a parabolic function along the tooth width, as shown in Figure 2c for crack sections A-A, which can be recognized in Figure 2a. When the crack length is less than the whole tooth width:

$$q(z) = \begin{Bmatrix} q_0\sqrt{\frac{W_c - z}{W_c}}, & z \in [0, W_c] \\ 0 & z \in [W_c, W] \end{Bmatrix} \tag{15}$$

where W_c is the crack length, W is the whole tooth width, and q_o is the maximum crack depth (see Figure 2c). When the crack length extends through the whole tooth width:

$$q(z) = \sqrt{\frac{q_0^2 - q_2^2}{W}.z + q_0^2} \tag{16}$$

where q_2 is shown in Figure 2c.

The Hertzian contact stiffness K_h can be calculated as follows:

$$\frac{1}{K_h} = \frac{4\left(1-\nu^2\right)}{\pi EW} \tag{17}$$

Calculating the stiffness of a cracked pinion tooth due to bending, shear, and axial compression can lead us to the calculation of the total mesh stiffness for one meshing tooth pair.

$$K_{m1} = 1/\left(\frac{1}{K_{tp}} + \frac{1}{K_{fp}} + \frac{1}{K_{tg}} + \frac{1}{K_{fg}} + \frac{1}{K_h}\right) \tag{18}$$

where K_{m1} is the total mesh stiffness for the first tooth pair. In cases where there are two tooth pairs in contact, the same calculations are repeated for the second tooth pair to find K_{m2}. Then we can obtain the equivalent mesh stiffness as follows:

$$K_m = K_{m1} + K_{m2} \quad (19)$$

The meshing stiffness representing the alternative process between single and double-tooth engagements is shown in Figure 3. In this figure, it is noted that when tooth cracks are introduced, distinct reductions in stiffness are observed. Figure 3 shows that the mesh stiffness is particularly dependent on crack propagation.

The parameters used in the gear modeling are given in Table 2.

Table 2. Material properties.

Young's modulus (GPa)	210
Poisson's ratio	0.3
Number of teeth, N	25
Pressure angle (°)	20
Pitch radiuses, R_1 and R_2 (mm)	11.9

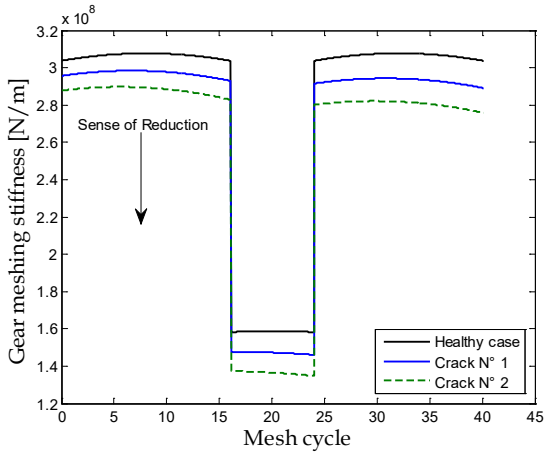

Figure 3. Total gear mesh stiffness for the different crack propagation

2.3. Model Simulation

The signal for gear transmission is essentially composed of the gear meshing frequency, their shaft rotation frequency, and their harmonics, which dominate the meshing vibration spectrum. However, when a tooth crack manifests itself, a short-duration impact will temporarily modify the vibration signal, and then the regular components of the signal become redundant for fault detection and monitoring in the context of predictive maintenance. Thus, by removing the regular components from the signal, the fault features can be efficiently detected and characterized. It is evident that the values of the statistical indicators applied to the residual signals increase significantly due to the presence of a tooth crack.

The dynamic response is calculated using a Newmark integration scheme. Then we deliberately introduced a defect in the shape of a crack in a gear tooth. The signal representing this response is shown in Figure 4.

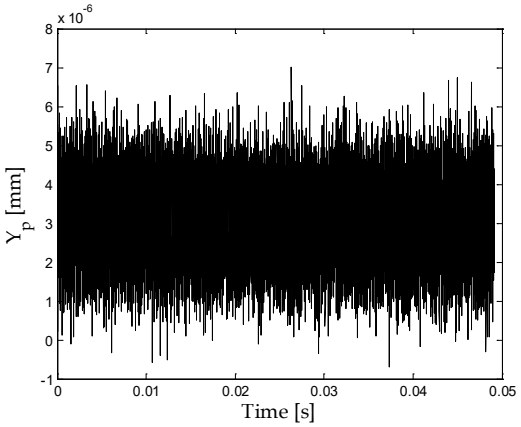

Figure 4. Original signal with crack depth = 0.8 mm

3. EVALUATING THE PERFORMANCE OF DENOISING ALGORITHMS

To evaluate the performance of our approach, we compared it with other algorithms by choosing these parameters: MAE, SNR, and PSNR. These widely used metrics in the literature have been chosen because we wanted the denoising algorithms to be not only accurate but also quick, so that real-time diagnostics could be performed. Each of the metrics is briefly explained below.

3.1. Mean Absolute Error (MAE)

MAE is a measure used to evaluate the relevance of denoising. Denoising is considered better if the MAE value is low. MAE is defined as follows:

$$MAE = \frac{\sum_{n=1}^{N}[x(n) - \tilde{x}(n)]}{N} \quad (20)$$

Let x(n) represent the original signal, $\tilde{x}(n)$ represent the de-noised signal, and N represent the length of the signal. Let 'n' represent the sample number, where n =1, 2, 3..N.

3.2. Signal to Noise Ratio (SNR)

SNR is a measure widely used to evaluate the performance of denoising methods. Denoising is considered better if the SNR value is high. SNR is given by the following formula:

$$SNR = 10\log_{10}\frac{\sum_{n=1}^{N} x(n)^2}{\sum_{n=1}^{N}[x(n) - \tilde{x}(n)]^2} \quad (21)$$

3.3. Peak Signal-to-Noise Ratio (PSNR)

The higher the value of the PSNR, the more relevant the denoising. The PSNR can be defined as:

$$PSNR = 20\log_{10}\frac{\max[x(n)]}{RMSE} \quad (22)$$

where RMSE is the square root of MSE.

4. RESULTS AND DISCUSSION

The study of the wavelet choice will be essentially based on a test of a wavelet variety. In this test, we compare MAE, SNR, and PSNR between the original signal and the reconstructed signal. Our choice will be focused on analyzing the wavelet, which will give the best values. The most used wavelets are Daubechies (db) and Symelets (sym). The noisy signal is represented in Figure 4. Firstly, this signal is denoised using a multi-resolution approach with soft and hard thresholding. After a multitude of simulations, the results recommend the following parameters: the family of wavelets (db9) and level 4 are selected. These conclusions have been minutely deduced from the results shown in Figures 5 and 6.

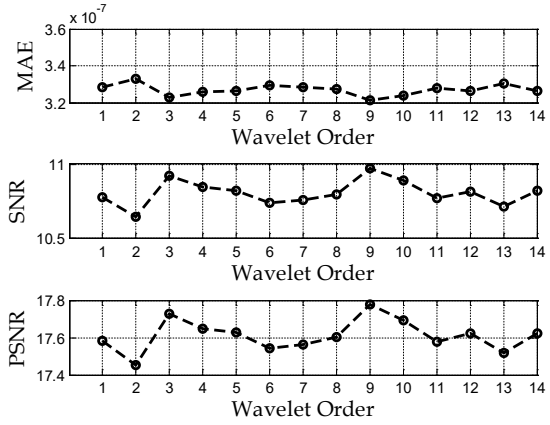

Figure 5. MAE, SNR, and PSNR vs different Wavelet Order

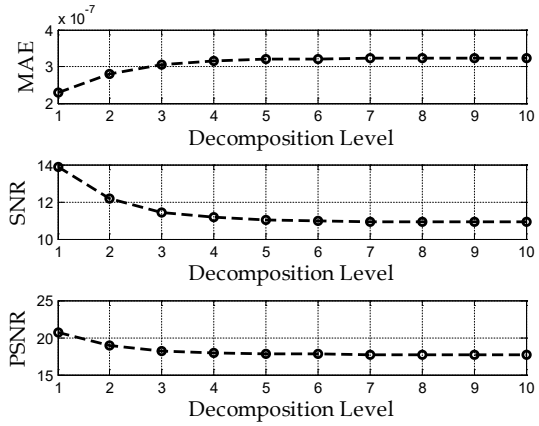

Figure 6. MAE, SNR, and PSNR vs different decomposition Level

In this section, the performance of various standard thresholding methods, namely Minimaxi, Sqtwolog, Rigrsure, and Heursure, is presented for denoising simulated signals corrupted by white Gaussian noise (SNR = -5 dB). The effect of various levels of decomposition is investigated on the performance of various thresholding estimation methods. The denoising of the signal using one of the thresholds below is obtained from the signal decomposition at level 6 by the (db9) wavelet.

4.1. Rigrsure

It is a soft threshold evaluator of unbiased risk. Suppose $W = \{w_1, w_2, w_3, ..., w_N\}$ a vector consists of the square of wavelet coefficients from small to large. Select the minimum value $r_b(b^{th}r)$ from the risk vector, which is given as [19]:

$$R = \{r_i\}_{i=1,...,N} = \frac{[N - 2i + (N-i)\omega_i] + \sum_{k=1}^{l}\omega_k}{N} \quad (23)$$

as the risk value. The selected threshold is $\lambda = \sigma\sqrt{w_b}$ where, w_b is the b^{th} squared wavelet coefficient (coefficient at minimum risk) chosen from the vector W and σ is the standard deviation of the noisy signal.

4.2. Heursure

The threshold is selected using a combination of Sqtwolog and Rigrsure methods. If the signal-to-noise ratio is very small, the SURE method's estimation is poor. In such a case, the fixed-form threshold of the Sqtwolog method gives better threshold estimation [19-20]. Let the threshold obtained from Sqtwolog method is λ_1 and the threshold obtained from Rigrsure is λ_2 then the Heuristic SURE gives the threshold given by:

$$\lambda = \begin{cases} \lambda_1 & A > B \\ \min(\lambda_1, \lambda_2) & A < B \end{cases} \quad (24)$$

where $A = \frac{s-N}{N}$ and $B = (\log_2 N)^{3/2}.\sqrt{N}$. The N is the length of the wavelet coefficient vector, and s is the sum of squared wavelet coefficients given as $s = \sum_{i=1}^{N} w_i^2$

4.3. Sqtwolog

For the universal threshold. The threshold values λ are calculated by the universal threshold (square root log) method given by [19]:

$$\lambda_j = \sigma_j\sqrt{2\log(N_j)} \quad (25)$$

where N_j is the length of the noisy signal at j^{th} scale and σ_j is the Median Absolute Deviation (MAD) at j^{th} scale given by:

$$\sigma_j = \frac{MAD_j}{0.6745} = \frac{median(|\omega|)}{0.6745} \quad (26)$$

where, ω represent wavelet coefficients at scale j.

4.4. Minimaxi

For minimax thresholding. This method finds the threshold (λ) using the Minimax principle. The threshold is given by [19]:

$$\lambda = \begin{cases} \sigma(0.3936 + 0.1829 \log_2 N) & N > 32 \\ 0 & N < 32 \end{cases} \quad (27)$$

4.5. Comparison MAE, SNR and PSNR at Soft and Hard Thresholding (SNR = -5 dB)

To optimize our multiresolution wavelet and transform algorithm, we performed several simulations to choose the best thresholding using performance indicators such as MAE, SNR, and PSNR. The results obtained are presented in the following figures.

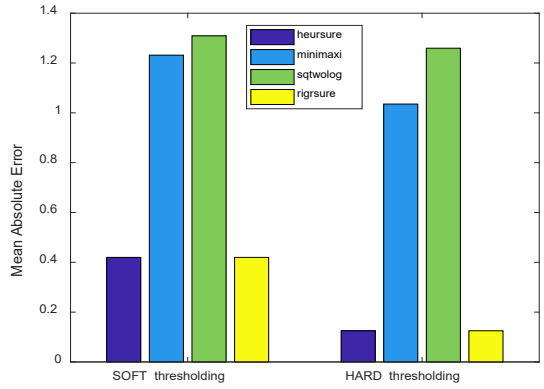

Figure 7. MAE comparison for soft and hard thresholding

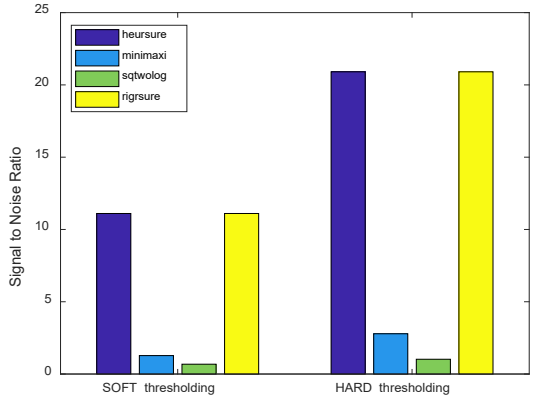

Figure 8. SNR comparison for soft and hard thresholding

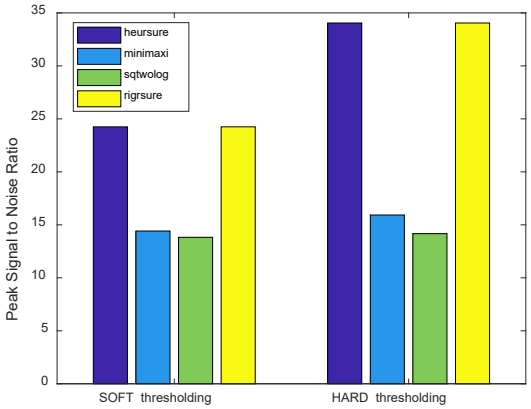

Figure 9. PSNR comparison for soft and hard thresholding

MAE, SNR, and PSNR values for the simulated signal are shown comparatively in Figures 7, 8 and 9. Lower levels of decomposition can be preferred for these methods. Also, the Rigrsure method has shown better performance as compared to the Heursure, Minimaxi, and Sqtwolog thresholding methods. Overall, from the results, the Rigrsure method of thresholding gives the best SNR and PSNR values compared with other thresholding methods for simulated signal denoising.

A second set of simulations was conducted to compare denoising by the wavelet transform with other very famous methods in the literature. The results obtained show that the performance of our chosen approach is better (see Table 3).

Table 3. Comparison MAE, SNR, and PSNR at different methods

	MAE	**SNR**	**PSNR**
Present Work	**0.1157**	**20.9055**	**34.0483**
Spectral Subtraction [21]	4.934210^{-6}	0	13.0573
Variable False Discovery Rate Approach [22]	1.4173	0.0076	11.9530
Morphological Techniques [23]	1.9534	-3.2186	9.7779

It is clear from Figure 10 that in the case of original signals, statistical indicators have increased considerably, highlighting a degradation of the gear condition. Kurtosis and the crest factor therefore always depend increasingly on the aggravation of the defect. From defect 5, the Kurtosis and Crest factors start to be higher, and their progression is substantially proportional to the amplitude of the defect.

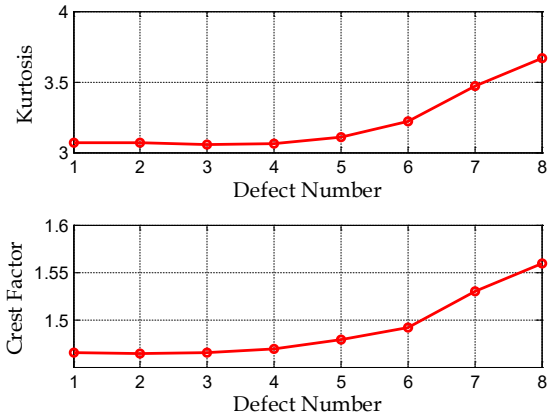

Figure 10. Kurtosis and Crest Factor evolution

Figure 11 clearly shows the contribution of the wavelet transform in the context of improving the sensitivity of the scalar indicators. When the size of the defect is very pronounced, we can also notice that the indicators do not vary linearly [24]. Indeed, the space-time between two successive shocks becomes inferior to the relaxation time, and the hypotheses on which the validity of the application is based are no longer confirmed by Pachaud [25]. The indicators studied become less than or equal to 3, so it can be concluded that they are no longer characteristic of an impulsive signal [21]. Figure 10 shows that in the context of conditional maintenance by the scalar indicators, the defect only appears when its value is 3.10 (in Figure 11, the order of the fault is 5). But an improvement in the sensitivity of this indicator by the proposed approach can help us detect its occurrence as early as possible.

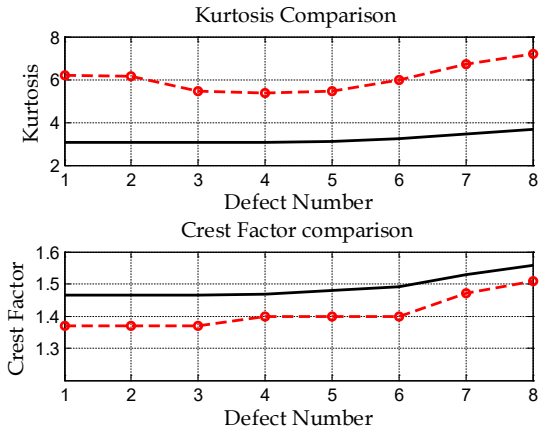

Figure 11. Comparison of original and reconstructed signals (Kurtosis and Crest Factor)

A comparison between the values of the scalars indicators considered in this paper before and after signal reconstruction (Figures 10 and 11) shows that the results are encouraging if one wants to detect faults in an early way because the indicators have been significantly improved, see Merzoug et al. [26].

5. CONCLUSION

This work aimed to evaluate denoising schemes based on wavelets for the denoising of simulated vibratory signal devices. Firstly, the denoising schemes were selected from an in-depth study of the literature in the field of denoising.

The denoising scheme based on the wavelet transform is widely used as a denoising scheme for gear vibration signals. On the other hand, the chosen approach was compared to two other schemes, and WT-based denoised signals can effectively identify gear faults. Based on SNR, Kurtosis, and MAE, the denoising scheme gives good results.

Furthermore, the performances of these schemes were evaluated, considering the characteristics extracted from the denoised signals. Among all WT schemes, the best denoising results were obtained. Thus, the wavelet transform can be retained as the best denoising scheme for gear vibration signals.

Finally, the findings from this study will provide insight into the selection of an appropriate mother wavelet by using different wavelet selection criteria. The performance of this denoising system should be evaluated based on the performance of Artificial Neural Network models (ANN). Features extracted from denoised signals will be used to train and test ANN models.

ACKNOWLEDGMENTS

The author would like to thank Saoudi Toufik for his support and cooperation. Toufik's professionalism, enthusiasm, and willingness to go beyond assisting us have been crucial in executing this study successfully.

REFERENCES

[1] Prasad SR, V., Poulose J., & Sadique A., Fault Detection of Spur Gear Using Machine Learning, *Proceedings of the International Conference on Aerospace & Mechanical Engineering (ICAME 21), March 3, 2022*.

[2] Meng Z., Shi G., & Wang F., Vibration response and fault characteristics analysis of gear based on time-varying mesh stiffness, *Mechanism and Machine Theory*, 2020, *148*, 103786.

[3] Marafona J. D., Marques P. M., Martins R. C., & Seabra J. H., Mesh stiffness models for cylindrical gears: A detailed review, *Mechanism and Machine Theory*, 2021, *166*, 104472.

[4] Xie C., & Shu X., A new mesh stiffness model for modified spur gears with coupling tooth and body flexibility effects, *Applied Mathematical Modelling*, 2021, *91*, 1194-1210.

[5] Wang Q., Chen K., Zhao B., Ma H., & Kong X., An analytical-finite-element method for calculating mesh stiffness of spur gear pairs with complicated foundation and crack, *Engineering Failure Analysis*, 2018, *94*, 339-353.

[6] Zhiguo W., Hongrui C., Yanyang Z., Wangpeng H., Yimin C., Mesh stiffness calculation using an accumulated integral potential energy method and dynamic analysis of helical gears, *Mechanism and Machine Theory*, 2015, Volume 92, 447-463,

[7] Wang S., & Zhu R., An improved mesh stiffness calculation model for cracked helical gear pair with spatial crack propagation path, *Mechanical Systems and Signal Processing*, 2022,*172*, 108989.

[8] Yang L., Wang L., Yu W., & Shao Y., Investigation of tooth crack opening state on time varying meshing stiffness and dynamic response of spur gear pair, *Engineering Failure Analysis*, 2021,*121*, 105181.

[9] Pandya Y., and Anand P., Simulation of crack propagation in spur gear tooth for different gear parameter and its influence on mesh stiffness, *Engineering Failure Analysis,* 2013, 30, 124-137.

[10] Pandya Y., and Anand P., Failure path based modified gear mesh stiffness for spur gear pair with tooth root crack, *Engineering Failure Analysi*s, 2013, 27, 286-296.

[11] Tayachi H., Gabzili H., & Lachiri Z., A New Approach for Detection of Gear Defects using a Discrete Wavelet Transform and Fast Empirical Mode Decomposition, *Int. J. Comput. Sci. Netw. Secur,* 2022, *22*, 123-130.

[12] He W., Hu J., Chen B., & Guo B., GMC sparse enhancement diagnostic method based on the tunable Q-factor wavelet transform for detecting faults in rotating machines, *Measurement*, 2021, *174*, 109001.

[13] Rajabi S., Azari M. S., Santini S., & Flammini F., Fault diagnosis in industrial rotating equipment based on permutation entropy, signal processing and multi-output neuro-fuzzy classifier, *Expert systems with applications*, 2022, *206*, 117754.

[14] Cai Z., Dang Z., Wen M., Lv Y., & Duan H., Application of compressed sensing based on adaptive dynamic mode decomposition in signal transmission and fault extraction of bearing signal, *Machines*, 2022, *10* (5), 353.

[15] Wang L., He J., Xiao H., Zeng Q., Ding X., & Shao Y., Joint suppression of normal gear mesh component and background noise for early local fault detection based on dynamic evolutionary digital filter, *Measurement*, 2022, *201*, 111711.

[16] Farag K.O., Kamal A.F.M., and Samir E., Mathematical modeling of gearbox including defects with experimental verification, *Journal of Vibration and Control*, 2012, 18(9), 1310-1321.

[17] Omar D. M., Rantatalo M., Aidanpää J.-O., Dynamic Modelling of a One-Stage Spur Gear System and Vibration-Based Tooth Crack Detection Analysis, *Mechanical Systems and Signal Processing,* 2015, 54-55, 293-305.

[18] Chen Z. & Shao Y., Dynamic simulation of spur gear with tooth root crack propagating along tooth width and crack depth, *Engineering Failure Analysis,* 2011, 18(8), 2149-2164.

[19] Verma N., Verma A. K., Performance analysis of wavelet thresholding methods in denoising of audio signals of some indian musical instruments, International *Journal of Engineering Science and Technology (IJEST)*, 2012, 4 (05), 2047-2052.

[20] Wang G.Y., Zhao X. Q., Wang X., Speech Enhancement Based on the Combination of Spectral Subtraction and Wavelet Thresholding, *International Conference on Apperceiving Computing and Intelligence Analysis*, 2009, 136-139.

[21] Esfandiar Z., Berouti Spectral Subtraction (https://www.mathworks.com/matlabcentral/fileexchange/7653-berouti-spectral-subtraction), MATLAB Central File Exchange. Retrieved February 22, 2023.

[22] Samer., Denoising using a variable False Discovery Rate Approach (https://www.mathworks.com/matlabcentral/fileexchange/51021-denoising-using-a variable-false-discovery-rate-approach), MATLAB Central File Exchange. Retrieved February 22, 2023.

[23] Sundar A., Pahwa V., Das C., Deshmukh M. & Robinson N., A comprehensive assessment of the performance of modern algorithms for enhancement of digital volume pulse signals, *Int. J. Pharm. Med. Biol. Sci*, 2016, 5, 91–98.

[24] Tandon N., A comparison of some vibration parameters for the condition monitoring of rolling element bearings, *Measuremen*t, 1994, 12, 285-289.

[25] Pachaud C., Crest factor and kurtosis contributions to identify defects inducing periodical impulsive forces, *Mechanical Systems and Signal Processing*, 1997, 11, 903-916.

[26] Merzoug M., Ait-Shgir K., Miloudi A., Dron J. P., Improvement of the Sensitivity of the Scalar Indicators Using a De-noising Method by Wavelet Transform, *In Applied Mechanics, Behavior of Materials, and Engineering Systems, Springer International Publishing*, https://doi.org/10.1007/978-3-319-41468-3_19, 2017, 239-250.